High-resolution measurement of dielectronic recombination of lithiumlike Cu^{26+}

G. Kilgus, D. Habs, D. Schwalm, and A. Wolf
Physikalisches Institut der Universität Heidelberg, W-6900 Heidelberg, Germany and Max-Planck-Institut für Kernphysik, W-6900 Heidelberg, Germany

N. R. Badnell
Department of Physics, Auburn University, Auburn, Alabama 36849-5311

A. Müller*
Institut für Kernphysik, Universität Giessen, W-6300 Giessen, Germany
(Received 13 May 1992)

Energies and absolute cross sections for dielectronic recombination of lithiumlike Cu^{26+} via $\Delta N = 0$ and $\Delta N = 1$ resonances have been measured at the Heidelberg heavy-ion storage ring TSR employing the electron cooler as a target of free electrons. In particular, resonances associated with $2s \rightarrow 2p$ and $2s \rightarrow 3l$ excitations have been observed. Resonances due to the doubly excited states $1s^2 2p_{1/2} nl$ and $1s^2 2p_{3/2} nl$ could be resolved up to $n = 30$. Fine-structure components are partly resolved for the $1s^2 3l3l'$ resonances. The results are compared with theoretical calculations and show good agreement.

PACS number(s): 34.80.Kw

I. INTRODUCTION

When a free electron collisionally excites an ion, it may lose enough energy to be captured by the ion, which then finds itself in a doubly excited state. If this intermediate state decays radiatively below the first ionization threshold, the ion is stable against autoionization and dielectronic recombination (DR) has occurred. It is well known that DR is the dominant recombination process in hot and dilute plasmas [1,2] and is thus of importance for the understanding of the dynamics of, for example, the solar corona and fusion plasmas.

The cross section as a function of the center-of-mass (c.m.) energy E for DR from an initial state i via a doubly excited intermediate state d with a natural width small compared to E can be represented in good approximation by [2]

$$\sigma_d(E) = \hat{\sigma}_d \, L_d(E) \tag{1}$$

with the integrated cross section of state d,

$$\hat{\sigma}_d = \frac{2\pi\hbar\mathcal{R}}{E_d} \pi a_0^2 \frac{g_d}{2g_i} \frac{A_a(d\rightarrow i) \sum_f A_r(d\rightarrow f)}{\sum_k A_a(d\rightarrow k) + \sum_{f'} A_r(d\rightarrow f')}, \tag{2}$$

where E_d denotes the resonance energy, g_i and g_d are the statistical weights of the initial ionic core and of the intermediate state, A_a and A_r are autoionization and radiative decay rates, a_0 is the Bohr radius, $\mathcal{R}$ the Rydberg energy constant, and $L_d(E)$ is the Lorentzian line shape normalized to $\int L_d(E)\, dE = 1$. In the sums, k denotes *all* states which are attainable by autoionization of the intermediate state and f runs over all states below the first ionization threshold, while f' includes all states below d.

The total DR cross section is thus given by

$$\sigma(E) = \sum_d \sigma_d(E) , \tag{3}$$

where the sum runs over all intermediate states contributing at E. In the following we will sometimes use an energy-averaged DR cross section defined by

$$\bar{\sigma}(E, \Delta E) = \frac{1}{\Delta E} \int_{E-\Delta E/2}^{E+\Delta E/2} \sigma(E')\, dE' . \tag{4}$$

Precise high-resolution DR measurements have become possible only recently by employing a merged-beam technique where the ion beam is superimposed on a cold intense electron beam in collinear geometry. Andersen and co-workers [3] have applied this method to the investigation of dielectronic resonances of light multiply charged ions at c.m. energies of the order of 10 eV and have obtained an energy spread as low as 0.1 eV. More recently this technique has been transferred by us to a heavy-ion cooler ring [4] using the electron cooler not only to cool the ion beam but also as an electron target. Very high ion energies have been employed, which significantly reduces the background from electron pickup in the residual gas. Together with the high intensity of the stored ion beam and the large detection efficiency for the charge-changed ions of close to 1, this technique results in a highly sensitive method, suited also for absolute measurements of small cross sections.

Earlier DR measurements [5] using Li-like ions in low charge states suffered from a low energy resolution so that no individual resonances could be observed. First high-resolution measurements on Li-like ions have been performed by Andersen, Bolko, and Kvistgaard [6] for elements up to oxygen, where the strong intrashell reso-

nances could be studied. These measurements are consistent with theoretical results taking into account a weak electric field of a few V/cm in the interaction region [7].

Here we report on DR measurements and calculations for a considerably heavier Li-like ion, namely Cu^{26+}; in particular we investigated the reactions channels

$$Cu^{26+}(1s^2 2s_{1/2}) + e^- \rightarrow \begin{cases} Cu^{25+}(1s^2 2p_{1/2} nl) & (n = 13, \ldots, \infty) \\ Cu^{25+}(1s^2 2p_{3/2} nl) & (n = 11, \ldots, \infty) \\ Cu^{25+}(1s^2 3lnl') & (n = 3, \ldots, \infty), \end{cases} \quad (5)$$

which constitute the dominant contributions to the DR cross section of Cu^{26+}. According to the excitation of the initially bound electron, the first two reactions are referred to as $\Delta N = 0$ or intrashell transitions, and the last one as $\Delta N = 1$ or intershell transitions. Regarding our theoretical calculations we followed Griffin and Pindzola [8], who have calculated DR cross sections for the Li-like ion Fe^{23+}, in particular to investigate field effects and to provide guidance for future experiments. Following their approach, we have calculated zero-field, intermediate coupling DR cross sections for Li-like copper ions using the AUTOSTRUCTURE package [9, 10].

In the following section, we shall describe the experimental setup and the measuring procedure. The data analysis is explained in Sec. III, while in Sec. IV the results are presented and compared to theoretical calculations.

II. EXPERIMENTAL TECHNIQUE

A. Setup

The principle of our procedure for measuring DR in a cooler storage ring is as follows (see also Fig. 1): The circulating ion beam is merged with the intense electron beam of the electron cooling device, the electron beam being guided by a longitudinal magnetic field. Those ions which capture an electron from the electron beam (or from the residual gas in this straight section) are separated from the main beam by the first bending magnet downstream of the cooler and are detected by a multichannel plate detector. In order to reveal the resonance-like behavior of the DR cross section with energy, the rate of charge-changed ions is recorded as a function of the relative energy between ions and electrons by altering the accelerating voltage of the electron gun.

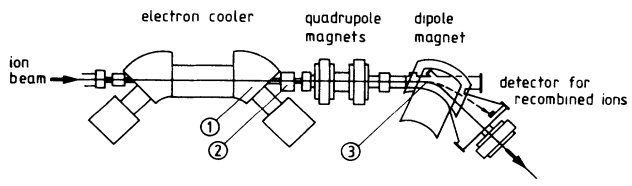

FIG. 1. Section of the TSR showing the electron-ion interaction zone and the detection zone for recombined ions. The numbers label sections with sizable transverse magnetic field resulting in motional electric fields (see text).

TABLE I. Relevant parameters of the TSR electron cooler.

Beam diameter	5.1 cm
Length of interaction zone	1.5 m
Cathode voltage (cooling)	4.9 kV
Electron current (cooling)	0.6 A
Cathode voltage (measurement)	1–9 kV
Electron current (measurement)	0.036–1.4 A
Electron density (measurement)	$7 \times 10^6 - 8 \times 10^7$ cm^{-3}
Guiding magnetic field	46 mT
Transverse temperature	0.1 eV
Minimum longitudinal temperature	4×10^{-4} eV

The measurements have been performed at the heavy-ion storage ring TSR [11] operated by the Max-Planck-Institut (MPI) für Kernphysik at Heidelberg. The beam of ^{63}Cu ions was supplied by the MPI tandem-booster facility. To obtain the required charge state of $q = 26$ with a reasonable abundance, the ions of mass m_i were passed through a final stripper foil after being accelerated to $E_i/m_i = 8.1$ MeV/u and were then injected into the ring with typical currents of up to 100 nA. The current in the ring was enhanced by a factor of about 10 using multiturn injection [12], storing successive beam pulses on adjacent orbits and thus filling the transverse phase space.

Electron cooling [13] of the circulating ions was achieved by matching the electron velocity with the ion velocity, which requires a kinetic energy for the electrons of 4.44 keV [hereafter referred to as the cooling energy $E_c = (m_e/m_i)E_i$]. Relevant parameters of the electron cooler are given in Table I and further details can be found in Ref. [14]. Within less than 1 s the ion-beam diameter decreases from initially 25 to 2 mm. Since the transverse phase space of the beam is now drastically reduced, new ions can be filled in by multiturn injection and cooled without disturbing the circulating beam. This so-called transverse electron-cooling stacking [12] increased the number of stored ions by another factor of 50, resulting in an ion current of typically 50 μA or 1.7×10^7 stored ions. The typical ion current is determined by the equilibrium between the rate of injected ions and the beam loss rate, which is mainly due to electron capture in the residual gas. Without reinjecting, the ion current decreased with a lifetime of about 1 min at an average ring vacuum of 5×10^{-11} mbar.

Ions having undergone a charge-changing reaction have a transverse distance from the main beam of 30 mm at the detector site and hit a 20-mm-diam multichannel plate (MCP) equipped with a metal anode. Since the size of the ion beam after cooling is only a few millimeters and the beam of charge-changed ions does not significantly change its width on its way to the detector, the active area of the MCP is large enough to collect all recombined ions. In order to check the efficiency of the MCP,

a $10 \times 10\,\mathrm{mm}^2$ Si surface-barrier detector was mounted below the MCP and could be moved into the beam of recombined ions. For the 8.1 MeV/u Cu^{25+} ions the detection efficiency was $(95 \pm 5)\%$.

B. Measuring procedure

The ion-beam preparation as described above was terminated after the beam intensity reached its equilibrium value. The electron energy was then changed in steps using a modulation technique: The cathode voltage was switched between a fixed and a variable level at a frequency of 15 Hz. This frequency was high enough to avoid pressure fluctuations due to the change of the electron current during one cycle. By scanning the variable voltage level, energy spectra were taken. The fast voltage changes were realized using a high-voltage amplifier whose output was added to the conventional cathode power-supply voltage.

Depending on the energy detuning of the electrons, the modulation of the electron energy served two purposes: Due to Coulomb collisions, the electrons exert a drag force [15] on the ions, whereby the ions are either accelerated for $v_e > v_i$ or decelerated for $v_e < v_i$. Here v_e and v_i denote the average electron and ion velocity, respectively. As this force is proportional to E^{-1} with E being the relative energy between ions and electrons, it is particularly strong for electron energies close to the cooling energy. In these cases special precautions have to be taken to avoid an energy shift of the ion beam during the DR measurement. For the measurements at very small relative energies (i.e., of the $\Delta N = 0$ resonances) the fixed voltage level could be chosen to be the cooling energy. When the voltage is set to the variable level ($v_e \gg v_i$) the ion energy starts to increase slowly. However, when it is reset to the fixed level ($v_e \lesssim v_i$) the ion energy is immediately reset to the cooling energy. This means that the ion velocity will stay very close to the electron velocity defined by the fixed level, provided the switching frequency between the two levels is high enough. The constancy of the ion energy was confirmed by observing the frequency spectra of the Schottky noise signal of the circulating beam. To reach relative energies beyond the voltage range of the high-voltage amplifier ($E \gtrsim 60\,\mathrm{eV}$), we employed a slightly different procedure. The fixed voltage level was set to a value where no resonances were present. Now the drag force is always positive and would result in a steady increase of the ion energy. The drag force was therefore compensated for using an induction accelerator [16] by which an adjustable constant force can be exerted on the ion beam. Again the constancy of the energy of the ion beam was checked using the Schottky noise signal.

At high relative energies (i.e., during the measurement of the $\Delta N = 1$ resonances at $E > 350\,\mathrm{eV}$) the drag force is so small that the change in ion energy is negligible for typical measuring intervals of 30 s. On the other hand, the signal-to-noise ratio is much smaller for the $\Delta N = 1$ resonances than for the $\Delta N = 0$ resonances, since the cross sections differ by at least one order of magnitude. Therefore the fixed level was set to a value near the resonances, where the background rate was measured. By scanning the variable level over the resonance region and taking the difference of both rates, background-subtracted spectra have been obtained.

III. DATA ANALYSIS

A. Evaluation of cross sections

From the recombination rate measured at an average electron-ion c.m. energy E_0, the experimental rate coefficient α can be deduced by

$$\alpha = R\gamma^2/\eta N_i n_e \,, \tag{6}$$

where R is the background-subtracted count rate, N_i denotes the number of stored ions, n_e is the electron density, and $\eta = 0.027$ is the ratio between the length of interaction zone, $L = 1.5\,\mathrm{m}$, and the ring circumference $C = 55.36\,\mathrm{m}$. The factor $\gamma^2 = [1 - (v_i/c)^2]^{-1}$ stems from the transformation between the c.m. and the laboratory frames and represents only a 2 % correction in the present experiment.

The number of stored ions was deduced from the relation $N_i = I_i C/qev_i$, with qe being the ion charge. The ion current I_i was measured by a dc beam-current transformer [17]. The electron density is connected with the electron current I_e by $n_e = I_e/Aev_e$, where A is the cross section of the electron beam. The electron current I_e was measured at the collector power supply. The determination of E_0 will be discussed in more detail in the next subsection.

The measured rate coefficient is related to the cross section by

$$\alpha(v_0) = \langle \sigma v \rangle = \int \sigma(v)\, v\, f(v_0, \mathbf{v})\, d^3v \,, \tag{7}$$

where $f(v_0, \mathbf{v})$ is the distribution of the electron velocity $\mathbf{v}$ relative to the ions around the average longitudinal c.m. velocity v_0 corresponding to the energy detuning E_0; in the nonrelativistic limit, $v_0 = (2E_0/m_e)^{1/2}$ because of $m_e \ll m_i$. If the variance of $f(v_0, \mathbf{v})$ is small compared to v_0, it is reasonable to deduce from the measured rate coefficient the energy-averaged experimental cross section by $\langle \sigma \rangle = \langle \sigma v \rangle / v_0$. For the cooled ion beams used in the present experiments and because of the large mass difference between electrons and ions, the velocity distribution function is dominated by the corresponding electron distribution, which can be described by a "flattened" Maxwellian [15] with different temperatures $T_\parallel$ and $T_\perp$ in the longitudinal and transverse direction:

$$f(v_0, \mathbf{v}) = \left(\frac{m_e}{2\pi k T_\parallel}\right)^{1/2} \exp\left[-\frac{m_e (v_\parallel - v_0)^2}{2kT_\parallel}\right] \times \frac{m_e}{2\pi k T_\perp} \exp\left(-\frac{m_e v_\perp^2}{2kT_\perp}\right) \,, \tag{8}$$

where k denotes the Boltzmann constant, $v_\parallel$ and $\mathbf{v}_\perp$ represent the longitudinal and transverse components of $\mathbf{v}$, and "flattened" refers to the fact that $T_\parallel \ll T_\perp$.

The natural widths of the DR resonances investigated in the present experiment are below 1 meV and thus much

smaller than the expected energy resolution. Under these conditions the measured rate coefficient due to a single DR resonance d reflects the electron velocity distribution and can be calculated analytically [18, 19] to yield

$$\alpha_d(v_0) = \frac{\hat{\sigma}_d\, v_d}{m_e \sigma_\perp^2 \zeta} \exp\left(-\frac{v_d^2 - v_0^2\zeta^{-2}}{\sigma_\perp^2}\right) \times \left[\mathrm{erf}\left(\frac{v_0 + v_d\zeta^2}{\sigma_\parallel \zeta}\right) - \mathrm{erf}\left(\frac{v_0 - v_d\zeta^2}{\sigma_\parallel \zeta}\right)\right] \quad (9)$$

with

$$\int \alpha_d(v_0(E_0))\, dE_0 = \hat{\sigma}_d\, v_d\,. \quad (10)$$

Here v_d denotes the relative velocity corresponding to the resonance energy E_d, and $\sigma_{\parallel,\perp}$ and ζ are given by $\sigma_{\parallel,\perp} = (2kT_{\parallel,\perp}/m_e)^{1/2}$ and $\zeta = (1 - T_\parallel/T_\perp)^{1/2}$, respectively. At the given values of $T_\parallel$ and $T_\perp$ (see Table I) the profile exhibits [6] a strongly asymmetric shape for $E_d < 10\,\mathrm{eV}$. Therefore, fitting the line profile given by Eq. (9) to the measured profile yields the transverse and the longitudinal temperature of the electron beam as well as the resonance energy, which, however, does not generally coincide with the center of gravity of the profile. For higher resonance energies the shape becomes more and more Gaussian around E_d with a full width at half maximum (FWHM) given by $\Delta E(\mathrm{FWHM}) = 4(E_d\, kT_\parallel \ln 2)^{1/2}$.

B. Determination of energies

The electron c.m. energy is given in the nonrelativistic limit by

$$E_0 = \left(\sqrt{E_e} - \sqrt{E_c}\right)^2, \quad (11)$$

where E_e is the average kinetic energy of the electrons and E_c is the cooling energy defined earlier. Equation (11) is useful for estimates, but for our analysis we used the relativistically correct expression:

$$E_0 = \left[\left(E_i + E_e + m_i c^2 + m_e c^2\right)^2 - \left(\sqrt{E_i^2 + 2m_i c^2 E_i} + \sqrt{E_e^2 + 2m_e c^2 E_e}\right)^2\right]^{1/2} - m_i c^2 - m_e c^2 \quad (12)$$

and

$$v_0 = (v_e - v_i)\left(1 + |v_i v_e|/c^2\right)^{-1} \quad (13)$$

with

$$v_{i,e} = c\left[1 - \left(1 + E_{i,e}/m_{i,e}c^2\right)^{-2}\right]^{1/2}. \quad (14)$$

The kinetic energy of the ions was determined by frequency-analyzing the Schottky noise signal of the circulating beam, which provides the average revolution frequency of the ions. An absolute energy calibration was performed with the help of the injection energy which was measured with an accuracy of 10^{-4} using a calibrated analyzing magnet.

The kinetic energy of the electrons in the beam is not uniform over its cross section but depends on the radial position because of the electron space charge. Since the cathode is operated in space-charge limited emission and the guiding magnetic field prevents the electron beam from blowing up, the current density distribution is homogeneous. We can thus write the kinetic energy in the center of the beam as

$$E_e = eU_{\mathrm{cath}} - eU_{\mathrm{sp}} = eU_{\mathrm{cath}} - \frac{I_e r_e\, m_e c^2}{e v_e}\left[1 + 2\ln(b/a)\right], \quad (15)$$

where r_e is the classical electron radius, $m_e c^2$ the electron rest mass, $b = 20\,\mathrm{cm}$ the diameter of the beam tube, and $a = 5.1\,\mathrm{cm}$ the diameter of the electron beam. The calculation of U_{sp} has to be carried out recursively since v_e depends on U_{sp} via E_e. One obtains $U_{\mathrm{sp}} \approx 500\,\mathrm{V}$ for $I_e = 560\,\mathrm{mA}$ and a cathode voltage of $U_{\mathrm{cath}} = 5\,\mathrm{kV}$. The electric potential and hence the increase of the electron energy with respect to the electron-beam axis is proportional to the square of the radial position; the potential difference between the center and the edge of the beam amounts to $U_{\mathrm{sp}}/[1 + 2\ln(b/a)] \approx 180\,\mathrm{V}$ for the present parameters.

The radial dependence of the electron energy has important experimental consequences, as an ion traveling through the electron beam at a finite angle experiences a broader energy distribution. In order to minimize the energy spread one thus has to make sure that the ion and electron beam are perfectly aligned. Since the electron cooling force is maximal for optimally aligned beams, the force was measured and optimized with the help of the induction accelerator to ensure perfect alignment [16]. In order to ensure that the ion and the electron beam were concentric, so that Eq. (15) can be used for the space-charge correction, the relative position of the two beams was adjusted until the average electron energy seen by the circulating ions, and hence the energy of the cooled ions themselves, which was observed by the Schottky noise spectrum, assumed its minimum. For large detunings of the electron energy, a displacement of the electron beam occurs during its bending in the toroids because of centrifugal forces. Therefore, a dipole correction magnet inside the toroids, used to compensate for these forces, was retuned during the measurement in order to keep the electron beam aligned.

The value for the space charge potential as given in Eq. (15) is valid only if there are no residual gas ions present which may screen the electron space charge. In practice the intense electron beam can act like an ion trap in which residual gas molecules are first ionized and then confined to the beam volume, the space-charge potential, and the magnetic field leading to a radial and potential wells in front of the cathode and the collector to a longitudinal confinement. Under conditions where this ion trapping occurred, the space-charge potential and hence the electron energy showed strong fluctuations leading

to a considerable broadening of the observed DR resonances. Hence, all residual gas ions were removed continuously from the beam by clearing electrodes mounted in the collector-side toroid. Our signal for complete clearing was that an isolated DR resonance was not shifted within one-tenth of the linewidth to smaller energies by increasing the clearing voltage.

The error of the relative energy E_0 is only due to uncertainties in the electron energy as the ion energy could be determined accurately from the Schottky spectrum. The systematic error of the laboratory electron energy E_e mainly stems from the uncertainty of the exact position of the ion beam relative to the electron-beam axis after the alignment procedure described above and from the remaining steady-state density of thermal residual gas ions. The total systematic error of E_e is estimated to be $\pm 3\,\mathrm{eV}$ at $E_e = 9\,\mathrm{keV}$. Due to the nonlinear transformation [see Eq. (11)] this corresponds to a systematic error of the average c.m. energy E_0 of $\pm 1\,\mathrm{eV}$ at $E_0 = 400\,\mathrm{eV}$ and $\pm 0.3\,\mathrm{eV}$ at $E_0 = 10\,\mathrm{eV}$.

The absolute systematic error of the measured cross section is mainly determined by the detector efficiency, the uncertainties in the ion current measurement, and the inaccurate knowledge of the effective length L of the overlap region [cf. Eq. (6)]. The systematic error of the cross-section scale is estimated to be 20%, while the relative uncertainty in comparing values of the cross section measured at different energies is $\lesssim 5\%$.

IV. RESULTS AND DISCUSSION

A. $\Delta N = 0$ transitions

In Fig. 2 we show the measured and theoretical rate coefficients for recombination of Cu^{26+} with free electrons at low c.m. energy via $\Delta N = 0$ transitions. Two Rydberg series of DR resonances due to doubly excited intermediate states of the configurations $1s^2 2p_{1/2} nl$ and $1s^2 2p_{3/2} nl$ are resolved up to $n = 30$. The bumps near the series limits are composed of unresolved resonances up to $n \approx 100$. The nonresonant "background" which increases with decreasing energy is due to radiative recombination. The contribution from electron capture in the residual gas was determined by comparing the measured rate at $E_0 = 85\,\mathrm{eV}$ (i.e., above the $1s^2 2p_{3/2} nl$ series limit) with the corresponding calculated rate for radiative recombination, which is estimated to be accurate to within 10%. The difference between these rates (approximately 80% of the measured rate at $E_0 = 85\,\mathrm{eV}$) was attributed to electron capture from the residual gas and was subtracted in the experimental spectrum of Fig. 2.

The variation in resonance strength is remarkable. The $2p_{1/2} 13l$ resonances at $E \approx 0.7\,\mathrm{eV}$ have an integrated cross section of $5 \times 10^{-17}\,\mathrm{cm^2\,eV}$, while that of the $2p_{1/2} 29l$ resonances just amounts to $1 \times 10^{-19}\,\mathrm{cm^2\,eV}$. At the strongest resonance a count rate close to the maximum allowed by the detector of $\approx 5 \times 10^4\,\mathrm{s^{-1}}$ was obtained. At typical intensities of $I_i = 50\,\mu\mathrm{A}$ and $I_e = 560\,\mathrm{mA}$ the spectrum shown in Fig. 2 could be taken in only a few minutes.

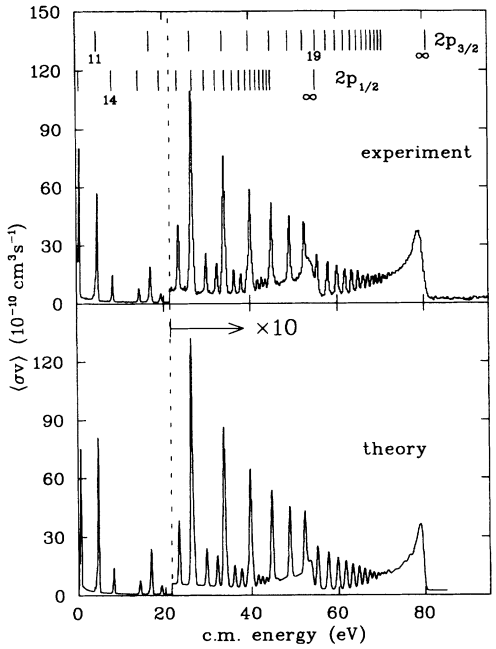

FIG. 2. Measured and calculated recombination rate coefficient for Cu^{26+} between 0 and 90 eV. Two Rydberg series of DR resonances ($1s^2 2p_{1/2} nl$ and $1s^2 2p_{3/2} nl$) appear on a nonresonant "background" due to radiative recombination. The theoretical rate coefficient was calculated with an electron velocity distribution characterized by $kT_\parallel = 6 \times 10^{-4}\,\mathrm{eV}$ and $kT_\perp = 0.1\,\mathrm{eV}$. The expected resonance energies and the principal quantum number n of the two series are indicated.

Neglecting the l spreading of the resonances for a given principal quantum number n, a simple Rydberg formula

$$E_n = E_{2p_{1/2},2p_{3/2}} - (26/n)^2\ \mathrm{Ry} \tag{16}$$

was fitted to the observed line energies with the threshold energy being the only free parameter. The deviations from the fit are smaller than 0.1 eV. The deduced threshold energies (statistical errors only) are $E_{2p_{1/2}} = 55.46(1)\,\mathrm{eV}$ and $E_{2p_{3/2}} = 80.95(2)\,\mathrm{eV}$, respectively, which have to be compared to more accurate plasma-spectroscopic data [20] of $E_{2p_{1/2}} = 55.159(3)\,\mathrm{eV}$ and $E_{2p_{3/2}} = 80.766(3)\,\mathrm{eV}$. The comparison indicates that our absolute energy scale is indeed accurate to better than 0.3 eV.

As discussed in Sec. III A the energy resolution is determined by the velocity distribution of the electron beam. In particular, the line profiles observed at energies below 10 eV should enable us to determine the longitudinal as well as the transverse electron beam temperature. Figure 3 shows the rate coefficient for the resonances $2p_{1/2} 14l$ at $E_0 = 8.35\,\mathrm{eV}$. Although the linewidths of the individual $14l$ states are negligible, the spreading of the different l states has to be taken into account for these low-n resonances. Thus we have fitted the data by three line profiles using relative resonance energies as given by theory. As expected, the longitudinal temperature is found to be much smaller than the transverse temperature. Owing to the residual l spreading, the extracted value of $kT_\parallel$ is only an upper limit. In fact, for higher-

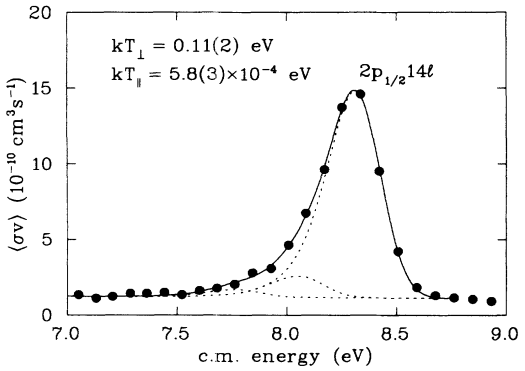

FIG. 3. Measured DR rate coefficient of the $2p_{1/2}14l$ resonances. The solid line is the result of a fit of three components (dashed lines) to the measured spectrum using Eq. (9) together with theoretical resonance energies and varying the transverse ($T_\perp$) and longitudinal ($T_\parallel$) temperature of the electron beam. The best fit results in the temperatures indicated.

lying resonances with negligible l-spreading longitudinal temperatures as low as 4×10^{-4} eV have been observed, corresponding to a resolution of ΔE(FWHM) = 0.2 eV at $E_0 \approx 50$ eV. The deduced transverse temperature of $kT_\perp = 0.11(2)$ eV is compatible with the cathode temperature of 0.105 eV (1220 K).

For the lowest-lying resonances $2p_{3/2}11l$ at 4.5 eV and $2p_{1/2}13l$ at 0.7 eV the splitting is already larger than the experimental linewidth, so that individual terms of these configurations can be observed, particularly those with small l, which strongly penetrate into the $1s^2$ core and are therefore more tightly bound. Figure 4(a) shows the measured rate coefficient for the $2p_{1/2}13l$ resonance, which exhibits four peaks at $E_0 \approx 0.15$, 0.35, 0.5, and 0.7 eV. The solid line is the theoretical cross section convoluted with the electron velocity distribution, while the dashed line describes the calculated contribution from radiative recombination. The radiative recombination rate was calculated with the distorted wave, LS coupling approximation [9, 21] for final states of an orbital angular momentum l up to 2 and from hydrogenic wave functions [22] for higher l, summing over final states up to $n = 90$ according to the experimental cutoff $n_{\rm cut}$ discussed below. The absolute heights of the resonances are well reproduced. The slight shift in energy, remaining within the estimated systematic error of ≈ 0.1 eV, may be due to the influence of the electron drag force (see Sec. II B) which is rather strong at this small c.m. energy. The theoretical cross section used for calculating the solid line in Fig. 4(a) is displayed in Fig. 4(b). The energy-averaged cross section according to Eq. (4) is represented for an energy bin of $\Delta E = 0.002$ eV, which allows the observed structure to be identified. The bump at 0.15 eV is produced by the $J = 0$ and 1 terms of the configuration $2p_{1/2}13s$. Moreover, the splitting of the $2p_{1/2}13p$ configuration is large enough that one can experimentally distinguish the state $2p_{1/2}13p_{1/2}(J = 1)$ at 0.35 eV from the remaining states centered around 0.5 eV. All contributions involving higher angular momenta are hidden in the dominant peak.

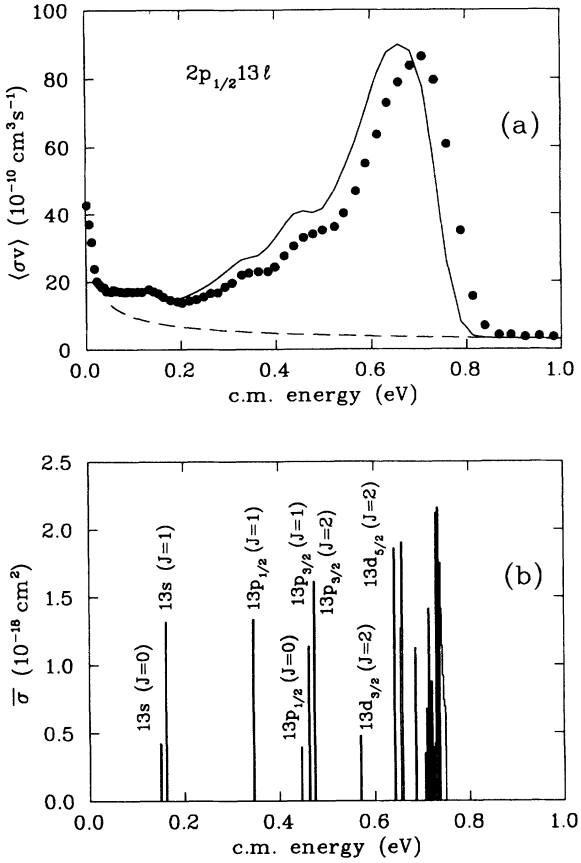

FIG. 4. (a) Measured rate coefficient near threshold. The solid line represents the theoretical rate coefficient assuming an electron velocity distribution characterized by $kT_\perp = 0.1$ eV and $kT_\parallel = 6 \times 10^{-4}$ eV. The dashed line shows the contribution due to calculated radiative recombination (see also the text). (b) Theoretical cross section averaged over energy bins of $\Delta E = 0.002$ eV.

We note that the sharp increase of the rate coefficient near threshold is probably not due to radiative recombination alone. The calculated rate coefficient for radiative recombination at $E_0 = 0$ for $T_\perp = 0.10$ eV amounts to only 25×10^{-10} cm^3 s^{-1}, which is about half the observed value. The excess rate may be explained by collisional-radiative recombination, which is the net effect of three-body recombination, impact ionization, collisional deexcitation, collisional excitation, and radiative deexcitation [23–25]. From elaborate numerical calculations [24] (with the proper Z scaling) and from a simplified treatment [25] one derives an additional rate coefficient at $E_0 = 0$ of about 20×10^{-10} cm^3 s^{-1}, which would account for the excess rate. It should be noted, however, that these calculations were done assuming quasi-steady-state conditions or even Saha equilibrium, which are problematic assumptions for the plasma conditions in the merged beams with an electron temperature of ≈ 0.1 eV and an interaction time between ions and electrons of only ≈ 40 ns.

A comparison between the integrated experimental cross section and the result of our theoretical calculation is shown in Fig. 5. The open circles are deduced

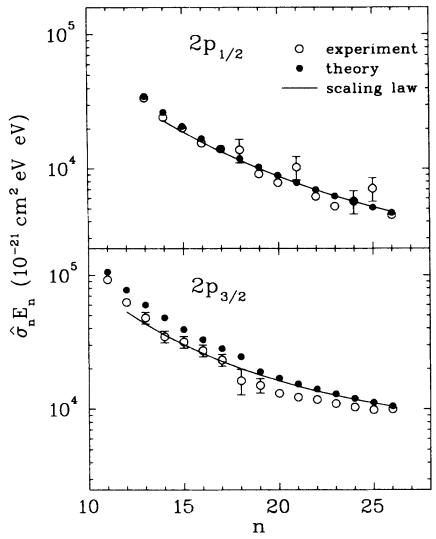

FIG. 5. Energy-integrated, l-summed cross section for the $2p_{1/2}nl$ and $2p_{3/2}nl$ resonances as a function of the principal quantum number n. To eliminate the trivial energy dependence of the DR cross section, the quantity (integrated cross section) × (resonance energy) is plotted. The larger error bars occur when resonances from different Rydberg series overlap.

from the measured rate coefficients for a given n after integration over the experimental line shape [see Eq. (10)]. The full circles represent the sum of the energy-integrated theoretical cross section for a particular principal quantum number. To eliminate the trivial energy dependence ($\sigma \propto E^{-1}$) of the DR cross section we have plotted the quantity (integrated cross section) × (resonance energy) versus the principal quantum number n, which thus reflects the n dependence of the matrix elements.

In order to describe the observed n dependence of $\hat{\sigma}_n E_n$ we have to consider all possible decay channels of the doubly excited states. The stabilizing radiative channels are

$$1s^2 2snl + h\nu \qquad (17)$$

$$1s^2 2pnl \nearrow \quad \searrow$$

$$1s^2 2pn'l' + h\nu', \quad l' = l \pm 1, \qquad (18)$$

where the final state in Eq. (18) is stable when $n' \leq 12\,(10)$ for $2p_{1/2}\,(2p_{3/2})$. These stabilization channels compete with the autoionization to the ground state; moreover, for the states $2p_{3/2}nl$ also the Auger channel $\rightarrow 2p_{1/2} + e^-$ opens up for $n \geq 19$. Neglecting Rydberg stabilization [Eq. (18)] one would expect according to Eq. (2) a DR cross section depending on n only weakly, as the autoionization rate for not too high l, $A_a(2p_{3/2}nl \rightarrow 2s + e^-)$, is much larger than the radiative rates for the inner stabilization [Eq. (17)], which amount to $A_r(2p_{1/2} \rightarrow 2s) = 2.1 \times 10^9\,\mathrm{s}^{-1}$ and $A_r(2p_{3/2} \rightarrow 2s) = 6.6 \times 10^9\,\mathrm{s}^{-1}$, respectively. Only a slow decrease of the cross section as a function of n, caused by the strong suppression of the autoionization rate above a critical l, is expected [26]. Thus, the observed *strong* decrease of $\hat{\sigma}_n E_n$ with n indicates the importance of the radiative transitions of the Rydberg electron. Indeed, taking for example $n = 15$, the total radiative rate to states with $n' = 2, \ldots, 10$ is 10^{10}–$10^{11}\,\mathrm{s}^{-1}$ and decreases approximately with n^{-3}.

The results of our detailed theoretical calculations using the AUTOSTRUCTURE package [9, 10] agree well with experiment for the $2p_{1/2}$ series, while the measured cross sections of the $2p_{3/2}$ series seem to be systematically lower than theoretically expected by 10–20 %. Thus, the ratio of the rates for the two series shows a slight but significant deviation from the theoretical prediction.

The successful description of the cross section of Rydberg states in the DR of H-like oxygen [4] by a simple scaling law [27] suggests the application of a similar scaling to the $\Delta N = 0$ Rydberg series observed here. For the n and l dependence of the decay rates in Eq. (2) we assume $A_a = a/n^3$ for $l \leq l_{\max}$, $A_a = 0$ for $l > l_{\max}$, $A_r(2p \rightarrow 2s) = r$, and $A_r(nl \rightarrow n'l') = r'/n^3$ ($l' < 10$), where a, r, and r' are constants and $l_{\max}$ is a cutoff parameter. The additional Auger channel for $2p_{3/2}nl$ ($n \geq 19$) is neglected. From Eq. (2) one then obtains

$$\hat{\sigma}_n E_n = 8\pi^2 \hbar a_0^2 \mathcal{R}\,(l_{\max}+1)^2 a\,\frac{1+(n_r/n)^3}{n^3+n_a^3+n_r^3}\,, \qquad (19)$$

where the abbreviations $n_a^3 = a/r$ and $n_r^3 = r'/r$ have been used. The values for n_a and n_r have been adjusted manually to reproduce the shape of the curve and then the absolute height has been fitted to the data. In Fig. 5 the solid lines represent these curves for $n_a = 80$, $n_r = 34$ ($2p_{1/2}$ series) and $n_a = 60$, $n_r = 23$ ($2p_{3/2}$ series), respectively. The representation of the data by the scaling law is satisfactory, in particular if one takes into account that the neglected Auger channel leads to an additional decrease of the DR cross section for the states $2p_{3/2}nl$ with $n \geq 19$ by $\approx 20\%$. The fit yields the quantity $(l_{\max}+1)^2 a$ from which (with the given values for n_a and r) one can derive $l_{\max} = 5.2(8)$ and $l_{\max} = 6.2(9)$ for the $2p_{1/2}$ and $2p_{3/2}$ series, respectively. These values are consistent with theoretical estimates [28].

In earlier DR measurements involving high Rydberg states [26] it was observed that external electric and magnetic fields may influence the rate of recombined ions observed in a crossed- or merged-beams experiment. An electric field in the interaction region can lead to an enhancement of the DR cross section by mixing of the angular momentum states for each Rydberg quantum number n such as to open up new DR channels beyond the zero-field cutoff $l_{\max}$. Calculations by Griffin and Pindzola [8] for Li-like Fe^{23+} ions have shown that even fields of the order of 10^4 V/cm do not affect the cross section for the $\Delta N = 0$ resonances with $n \leq 20$. As in our experiment the maximum field strength is only about 10 V/cm in the center of the electron beam, we do not expect to observe an enhancement in the measured cross section, at least for those states individually resolved ($n \leq 30$). This is clearly confirmed by the good agreement between the data and the zero-field theoretical calculation according to Fig. 5. On the other hand, significant deviations between the measured and the calculated rate coefficient are

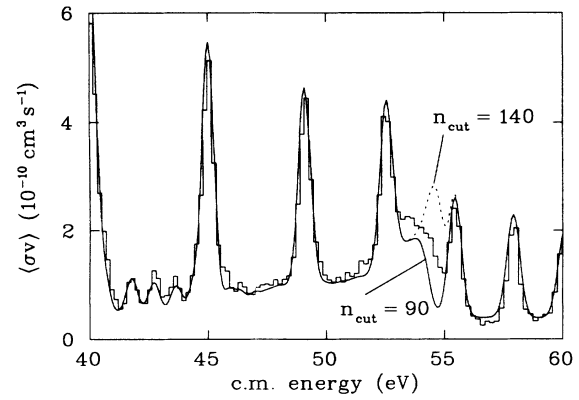

FIG. 6. DR rate coefficient in the region of the $2p_{1/2}$ series limit; the strong resonances belong to the $2p_{3/2}nl$ series. The histogram represents the measured rate coefficient and the smooth curves give the theoretical calculation at zero electric field for an electron velocity distribution characterized by $kT_\perp = 0.1\,\text{eV}$ and $kT_\parallel = 6 \times 10^{-4}\,\text{eV}$. The theoretical rate coefficient has been cut off at $n_{\text{cut}} = 90$ (solid curve) and $n_{\text{cut}} = 140$ (dashed curve).

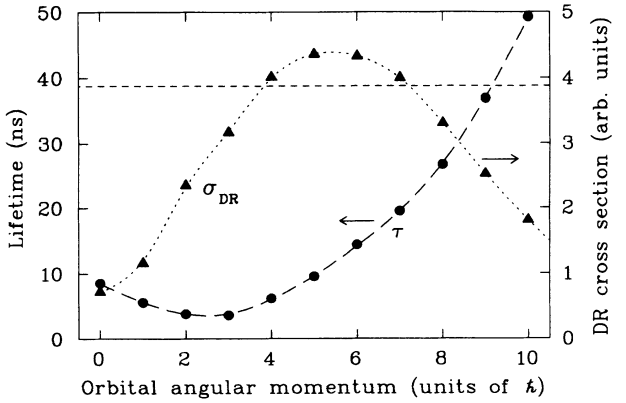

FIG. 7. Lifetime of Rydberg ions with $n = 100$ and a core charge of 26 as a function of the orbital angular momentum l (full circles) and contributions of l sublevels to the DR cross section [28] in arbitrary units (triangles). The dashed line denotes the time of flight of the circulating ions through the electron beam.

found in the energy range of the higher unresolved Rydberg resonances, in particular below the $2p_{1/2}$ threshold close to 55 eV. The rate coefficient in this energy range is shown in detail in Fig. 6. The histogram is the experimental result, whereas the solid and dashed lines represent theoretical zero-field calculations deliberately cut off at $n_{\text{cut}} = 90$ and 140, respectively. The data in the region of resonances with $n \gtrsim 45$ ($E > 52\,\text{eV}$) show an enhancement with respect to the calculated rate coefficient, which may be attributed to the electric field in the interaction region.

Very close to the excitation threshold, the observed DR rate coefficient is influenced also by the removal of weakly bound Rydberg electrons by field ionization in (motional) electric fields arising in the rest frame of the recombined ions on their way from the interaction zone to the detector. Since the reionized recombined systems cannot contribute to the measured rate, a cutoff principal quantum number n_{cut} is introduced in the theoretical calculation. By an electric field of strength F, all electrons in states above $n > n_{\text{str}}$ will be stripped off, with n_{str} given for hydrogenic systems by [29]

$$n_{\text{str}}^4 \simeq 6.8 \times 10^8\ \text{V/cm} \times q^3/F\,. \tag{20}$$

Substantial motional electric fields due to transverse magnetic fields appear in the toroid of the electron cooler (1), in a correction dipole (2), and in the bending magnet (3) as depicted in Fig. 1. The electric-field strengths and the corresponding critical quantum numbers n_{str} are $F^{(1)} = 8 \times 10^3$ V/cm, $n_{\text{str}}^{(1)} = 197$ in region (1), $F^{(2)} = 1 \times 10^4$ V/cm, $n_{\text{str}}^{(2)} = 186$ in region (2), and $F^{(3)} = 3 \times 10^5$ V/cm, $n_{\text{str}}^{(3)} = 80$ in region (3). On their way to these field regions, Rydberg ions formed in states $n > n_{\text{str}}$ can radiatively decay to states below n_{str} and thus stabilize against reionization. For this stabilization to occur, we require the mean radiative lifetime of the Rydberg state to be smaller than the travel time between the interaction region and the ionizing field; we denote by n_{life} the principal quantum number for which the lifetime just reaches the travel time. The effective critical quantum number n_{cut} is thus given by the larger value of n_{str} and n_{life}.

As seen from Fig. 6, the observed cutoff lies at $n_{\text{cut}} \approx 100$, corresponding approximately to $n_{\text{str}}^{(3)}$ for the bending magnet. On the other hand, the related travel time is 130 ns and a calculation of the radiative lifetime of the dominantly populated l states for $n = 100$ (see Fig. 7) shows that almost none of these ions are expected to remain in this Rydberg state until reaching the bending magnet. However, the observed $n_{\text{cut}} \approx n_{\text{str}}^{(3)}$ might be explained by a modification of the l distribution, which would lead to a longer average lifetime and reduce n_{life} to a value below $n_{\text{str}}^{(3)}$.

Two effects may be responsible for a modification of the l distribution. (i) Although the electric field of $\lesssim 10\,\text{V/cm}$ expected at the center of the electron beam

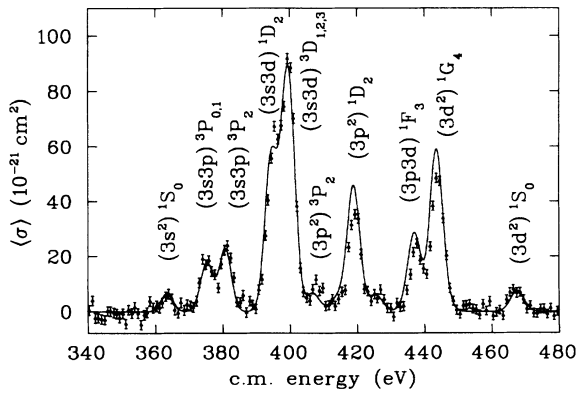

FIG. 8. Measured DR cross section for the LMM resonances ($1s^2 3l3l'$). The solid line represents the calculated cross section convoluted with the experimental resolution ($kT_\parallel = 4 \times 10^{-3}\,\text{eV}$).

is quite small, for very high n states it nevertheless mixes states of different l via the Stark effect. This l mixing on one hand leads to the field enhancement of the cross section as discussed above and on the other hand gives rise to the population of higher l states and a corresponding increase of the average lifetime of Rydberg levels with $n \gtrsim n_{\mathrm{str}}^{(3)}$. As simplified estimates show, the lifetime may indeed become long enough to account for the observed value of n_{cut}. (ii) Another process which may change the l distribution is the soft collision of an electron with a Rydberg ion. This effect has already been observed earlier in an experimental study of electron impact excitation of helium [30]. Scaling the cross section for this process given in Ref. [30] one can estimate that a Rydberg ion with $n = 100$ suffers on the average three l-changing collisions within the interaction region. Al-

TABLE II. Comparison of experimental and theoretical resonance energies E_d and integrated cross sections $\hat{\sigma}_d$. The experimental cross sections have been obtained by fitting Gaussian functions to the measured spectrum. The column Σ (theory) sums up the contributions which lie inside one experimental linewidth. The errors given are only statistical.

	E_d (eV)		$\hat{\sigma}_d$ (10^{-21} cm^{2}eV)		
Term	Theory	Experiment	Theory	Σ (theory)	Experiment
$3s^2\ {}^1S_0$	363.3	363.4(5)	28.3	28.3	24(5)
$3s3p\ {}^3P_0$	374.0		20.8		
$3s3p\ {}^3P_1$	375.7	375.8(2)	61.5	82.3	89(5)
$3s3p\ {}^3P_2$	380.9	381.3(2)	100.1	100.1	106(6)
$3s3p\ {}^1P_1$	393.6		61.6		
$3s3d\ {}^1D_2$	394.7	395.1(1)	192.1	253.7	275(8)
$3s3d\ {}^3D_1$	398.1		92.9		
$3p^2\ {}^3P_0$	398.4		2.1		
$3s3d\ {}^3D_2$	399.1		143.0		
$3s3d\ {}^3D_3$	400.3	399.8(1)	211.0	449.0	412(6)
$3p^2\ {}^3P_1$	402.4		< 0.1		
$3p^2\ {}^3P_2$	406.7		29.5		
$3p3d\ {}^3F_2$	410.0	408.2(3)	4.6	34.1	46(5)
$3p3d\ {}^3F_3$	414.2	413.7(9)	21.1	21.1	12(5)
$3p3d\ {}^1D_2$	416.2		5.0		
$3p^2\ {}^1S_0$	418.8		7.3		
$3p3d\ {}^3F_4$	419.0		10.2		
$3p^2\ {}^1D_2$	419.0		190.6		
$3p3d\ {}^3D_1$	419.8		1.6		
$3p3d\ {}^3D_2$	421.7	419.3(1)	2.0	211.7	168(5)
$3p3d\ {}^3D_3$	424.6		10.7		
$3p3d\ {}^3P_1$	425.7		6.5		
$3p3d\ {}^3P_0$	425.8		2.6		
$3p3d\ {}^3P_2$	426.3	426.4(4)	10.1	29.9	31(5)
$3d^2\ {}^3F_2$	433.0		2.6		
$3d^2\ {}^3F_3$	434.4		< 0.1		
$3d^2\ {}^3F_4$	436.1		24.2		
$3p3d\ {}^1F_3$	437.2	437.5(1)	114.0	138.2	106(5)
$3d^2\ {}^3P_0$	441.8		0.7		
$3d^2\ {}^3P_1$	442.6		< 0.1		
$3d^2\ {}^3P_2$	443.0		6.4		
$3d^2\ {}^1G_4$	443.5	444.0(1)	273.2	279.6	228(6)
$3p3d\ {}^1P_1$	445.1		< 0.1		
$3d^2\ {}^1D_2$	446.8		9.1		
$3d^2\ {}^1S_0$	467.6	467.1(3)	36.6	36.6	40(5)

though we do not know anything about the populated final states, high-l states are probably favored because of their higher statistical weight.

In order to arrive at a complete understanding of the behavior of Rydberg ions in the cooling section, the magnetic field of the cooler, as well as the time-dependent electric and magnetic fields in the ion rest frame caused by the toroid and the correction dipole, in addition to the already mentioned effects, should be considered.

B. $\Delta N = 1$ transitions

The strongest DR resonances in Li-like Cu besides the $\Delta N = 0$ transitions are resonances associated with the capture process

$$Cu^{26+}(1s^2 2s) + e^- \rightarrow Cu^{25+}(1s^2 3lnl') \,. \qquad (21)$$

The cross section for these processes is smaller than that for $\Delta N = 0$ resonances by typically one to two orders of magnitude. The excitation energies reach from 360 to 1485 eV (series limit). Figure 8 shows the part of the spectrum associated with a capture into $n = 3$, i.e., the LMM resonances. Eleven resonance peaks were resolved and identified by comparison with our theoretical result, given by the solid line. The observed linewidth is ΔE(FWHM) ≈ 4 eV and corresponds to an effective longitudinal temperature of $\approx 3.5 \times 10^{-3}$ eV, much larger than the one observed for the low-lying resonances. The linewidth in this measurement is determined by two effects. (i) When the ion- and electron-beam velocities are detuned permanently, the ion beam heats up because of intrabeam scattering, which results in a relative velocity spread of $\approx 1 \times 10^{-3}$ (FWHM). This spread contributes $\approx 2 \times 10^{-3}$ eV to the effective longitudinal temperature. (ii) A high electron current up to 1500 mA has been employed, which resulted in a sizable energy transfer from the hot transverse into the cold longitudinal motion of the electrons and contributed $\approx 1 \times 10^{-3}$ eV to the effective longitudinal temperature.

As seen by the double-peak structure near 380 eV, the experimental linewidth is small enough to resolve the fine-structure level $3s3p(^3P_2)$ from the rest of the triplet. All over the spectrum, good agreement between theory and experiment is found. A quantitative comparison of the measured resonance energies and cross sections with theory is given in Table II.

The high-lying members of the $3lnl'$ Rydberg series are shown in Fig. 9. Whereas in the measurements discussed so far the electrons were kept faster than the ions [$E_e > E_c$; see Eq. (11)], in order to use the strong increase of the electron density with the electron-beam energy, the c.m. energy range of the higher $\Delta N = 1$ resonances could not be reached in this mode because of technical limitations of the electron-beam energy and current. Therefore, the spectrum displayed in Fig. 9(a) was measured at small electron energy $E_e < E_c$ and offers less statistics because of the lower electron density. The Rydberg series $3lnl'$ can be followed up to $n = 10$. Then, the cross section drops owing to the fact that the dominant configurations $3dnl$ radiatively decay to the states $2pnl$, which lie above the ionization threshold for $n \geq 11$ (see

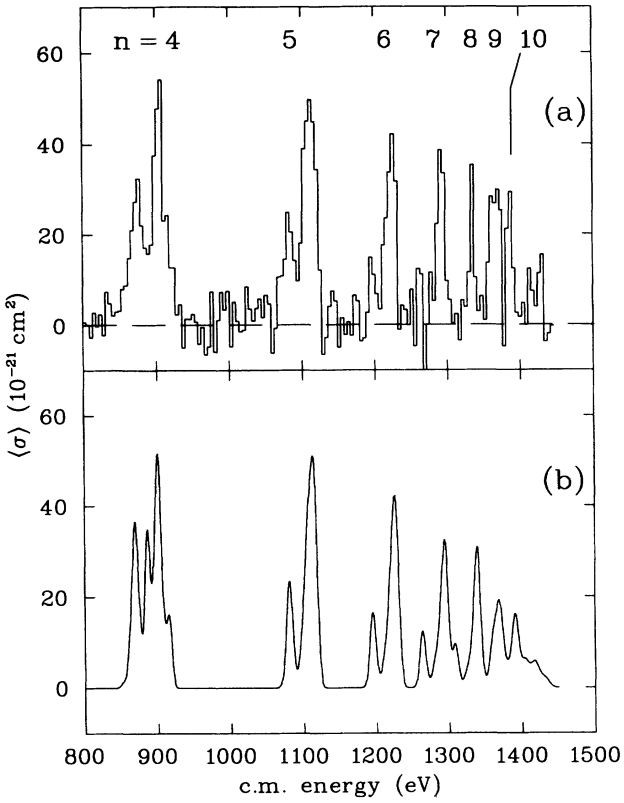

FIG. 9. (a) Measured and (b) calculated cross section for the $1s^2 3lnl'$ resonances. The theoretical cross section was convoluted with the experimental resolution ($kT_{\parallel} = 4 \times 10^{-3}$ eV).

Fig. 2) and thus can autoionize. Another feature of the spectrum is the double-peak structure with a splitting almost constant for the resonances $n = 4, \ldots, 7$. The low-energy peaks of these doublets are due to the configurations $3snl$, which have a slightly larger binding energy than the configurations $3pnl$ and $3dnl$ giving rise to the upper peaks. The theoretical calculation shown in Fig. 9(b) compares well, both in energy and absolute height, with the measured spectrum for $n \geq 5$, while for the $n = 4$ resonances a slight discrepancy in the energetical positions of the dominant contributions appears.

V. CONCLUSION

We have presented measured and calculated resonance energies and cross sections for dielectronic recombination of Li-like Cu^{26+} via intermediate states $1s^2 2pnl$ ($\Delta N = 0$ resonances) and $1s^2 3lnl'$ ($\Delta N = 1$ resonances). For the $\Delta N = 0$ resonances very high cross sections up to 10^{-16} cm^2 have been observed. The corresponding Rydberg series could be resolved up to $n = 30$. The integrated cross sections of the Rydberg resonances revealed the importance of the stabilization by radiative transitions of the Rydberg electron. The detailed comparison between theory and experiment shows good agreement. In the measured spectra for the $\Delta N = 1$ resonances at energies above 380 eV, the fine-structure components could be partly resolved. Again, theory and experiment are in good agreement.

These measurements represent a stringent test of the theory of dielectronic recombination for Li-like ions at high Z and suggest that the theoretical description is indeed very reliable. The issue for the future will be to investigate more complex ions, which are of particular interest in plasma physics and for which precise experimental data are still lacking.

ACKNOWLEDGMENTS

We would like to thank the TSR group, in particular E. Jaeschke and M. Grieser, for their support during the beam time. We also thank M. Pindzola for useful discussions and A. Lampert for his contributions in the final phase of this work. The experimental work has been funded by the German Federal Minister for Research and Technology (Bundesministerium für Forschung und Technologie) under Contract No. 06 HD 133 I and by the Gesellschaft für Schwerionenforschung (GSI), Darmstadt. The theoretical work was supported by a grant from the Office of Fusion Energy of the U.S. Department of Energy under Contract No. DE-FG05 86ER53217 with Auburn University.

* Present address: Institut für Strahlenphysik, Universität Stuttgart, W-7000 Stuttgart 80, Germany.

[1] A. Burgess, Astrophys. J. **139**, 776 (1964).
[2] B. W. Shore, Astrophys. J. **158**, 1205 (1969).
[3] L. H. Andersen, P. Hvelplund, H. Knudsen, and P. Kvistgaard, Phys. Rev. Lett. **62**, 2656 (1989).
[4] G. Kilgus, J. Berger, M. Grieser, D. Habs, B. Hochadel, E. Jaeschke, D. Krämer, R. Neumann, G. Neureither, W. Ott, D. Schwalm, M. Steck, R. Stokstad, E. Szmola, A. Wolf, R. Schuch, A. Müller, and M. Wagner, Phys. Rev. Lett. **64**, 737 (1990).
[5] P. F. Dittner, S. Datz, P. D. Miller, P. L. Pepmiller, and C. M. Fou, Phys. Rev. A **35**, 3668 (1987).
[6] L. H. Andersen, J. Bolko, and P. Kvistgaard, Phys. Rev. A **41**, 1293 (1990).
[7] D. C. Griffin, M. S. Pindzola, and P. Krylstedt Phys. Rev. A **40**, 6699 (1989).
[8] D. C. Griffin and M. S. Pindzola, Phys. Rev. A **35**, 2821 (1987).
[9] N. R. Badnell, J. Phys. B **19**, 3827 (1986).
[10] N. R. Badnell and M. S. Pindzola, Phys. Rev. A **39**, 1685 (1989).
[11] E. Jaeschke, D. Krämer, W. Arnold, G. Bisoffi, M. Blum, A. Friedrich, C. Geyer, M. Grieser, D. Habs, H.-W. Heyng, B. Holzer, R. Ihde, M. Jung, K. Matl, R. Neumann, A. Noda, W. Ott, B. Povh, R. Repnow, F. Schmitt, M. Steck, and E. Steffens, in *Proceedings of the European Particle Accelerator Conference, Rome, 1988*, edited by S. Tazzari (World Scientific, Singapore, 1989), p. 365.
[12] M. Grieser, M. Blum, D. Habs, R. v. Hahn, B. Hochadel, E. Jaeschke, C. M. Kleffner, M. Stampfer, M. Steck, and A. Noda, in *Proceedings of the 19th INS Symposium on Cooler Rings and Their Applications, Tokyo, 1990*, edited by T. Katayama and A. Noda (World Scientific, Singapore, 1991), p. 190.
[13] G. I. Budker and A. N. Skrinsky, Usp. Fiz. Nauk **124**, 561 (1978) [Sov. Phys. Usp. **21**, 277 (1978)].
[14] M. Steck, M. Blum, M. Grieser, E. Jaeschke, C. M. Kleffner, D. Krämer, W. Ott, and R. Repnow, in *Proceedings of the Workshop on Electron Cooling and New Cooling Techniques, Legnaro, 1990*, edited by L. Calabrese and L. Tecchio (World Scientific, Singapore, 1991), p. 64.
[15] H. Poth, Phys. Rep. **196**, 135 (1990).
[16] Ch. Ellert, D. Habs, E. Jaeschke, T. Kambara, M. Music, D. Schwalm, P. Sigray, and A. Wolf, Nucl. Instrum. Methods A **314**, 399 (1992).
[17] K. Unser, IEEE Trans. Nucl. Sci. **28**, 2344 (1981).
[18] G. Kilgus, doctoral thesis, University of Heidelberg, 1990.
[19] L. H. Andersen and J. Bolko, Phys. Rev. A **42**, 1184 (1990).
[20] J. Sugar and A. Musgrove, J. Phys. Chem. Ref. Data **19**, 527 (1990), and references therein.
[21] W. Eissner, M. Jones, and H. Nussbaumer, Comput. Phys. Commun. **8**, 270 (1974).
[22] A. Burgess, D. G. Hummer, and J. A. Tully, Philos. Trans. R. Soc. (London) Ser. A **266**, 225 (1970).
[23] D. R. Bates, A. E. Kingston, and R. W. P. McWirther, Proc. R. Soc. (London) Ser. A **267**, 297 (1962); **270**, 155 (1962).
[24] J. Stevefelt, J. Boulmer, and J.-F. Delpech, Phys. Rev. A **12**, 1246 (1975).
[25] H. F. Beyer, D. Liesen, and O. Guzman, Part. Accel. **24**, 163 (1989).
[26] A. Müller, D. S. Belić, B. D. DePaola, N. Djurić, G. H. Dunn, D. W. Mueller, and C. Timmer, Phys. Rev. A **36**, 599 (1987).
[27] Y. Hahn and K. J. LaGattuta, Phys. Rep. **166**, 195 (1988).
[28] N. R. Badnell, J. Phys. B **23**, L565 (1990).
[29] E. P. Kanter, D. Schneider, Z. Vager, D. S. Gemmell, B. S. Zabransky, Gu Yuan-zhuang, P. Arcuni, P. M. Koch, D. R. Mariani, and W. Van de Water, Phys. Rev. A **29**, 583 (1984).
[30] J. A. Schiavone, D. E. Donohue, D. R. Herrick, and R. S. Freund, Phys. Rev. A **16**, 48 (1977).